

An experimental and theoretical investigation into the binding interactions of silver cluster cations with ethene and propene

Manuel J. Manard, Paul R. Kemper, Michael T. Bowers*

Department of Chemistry & Biochemistry, University of California, Santa Barbara, CA 93106, United States

Received 10 November 2005; received in revised form 13 December 2005; accepted 13 December 2005

Available online 14 February 2006

Abstract

Sequential bond dissociation energies (BDEs) and association entropies for the attachment of C_2H_4 ligands to ground-state Ag_m^+ ($m=3-13$) clusters and for the attachment of C_3H_6 ligands to ground-state Ag_m^+ ($m=3-9$) clusters have been measured using temperature-dependent equilibrium methods. Variations in metal–ligand BDEs are examined in detail both as a function of sequential ligand addition to a given Ag_m^+ cluster and as a function Ag_m^+ cluster size for the first ligand additions. With the exception of the Ag_6^+ and Ag_7^+ clusters, BDEs for the loss of a ligand from the $Ag_m^+(L)$ ($m=3-13$, $L=C_2H_4$; $m=3-9$, $L=C_3H_6$) clusters decrease as the size of the silver clusters increase. Electronic structure calculations at the DFT-B3LYP level were performed in order to determine the vibrational frequencies, rotational constants and geometries of the silver–alkene clusters of interest as well as the nature of the bonding of these clusters and its variation with core ion coordination.

© 2005 Elsevier B.V. All rights reserved.

Keywords: Silver cluster cations; Ethene; Propene; Bond dissociation energies; DFT

1. Introduction

The chemistry of metal clusters has received considerable attention over the last 25 years [1–3]. This can be primarily attributed to the fact that the intrinsic properties of clusters are intermediate to those of atoms and the bulk-phase [4]. This region is of particular interest for coinage metals because it has been shown to be important in a number of catalytic reactions [5–7].

In order to elucidate the properties of these clusters, multiple experimental and theoretical investigations have focused on their interactions with small molecules [8–11]; H_2 [12–14], CO [15–17], O_2 [18,19] and polyatomic hydrocarbons [20–24]. These studies have provided fundamental information on metal cluster–ligand binding energies and geometries. Despite the wealth of information available on cluster–small molecule interactions, questions remain such as the size range of clusters responsible for catalytic action and where the transition to bulk-phase properties occurs.

In an attempt to provide further insight into these issues, a program has been initiated at UCSB in which the proper-

ties of size-selected transition metal clusters are studied both deposited on metal-oxides surfaces [25] and in the gas-phase. In the gas-phase, these investigations are primarily focused on the interactions of positively and negatively charged silver and gold clusters with ethene and propene [26–28]. This is due to the relatively recent discovery that Ag and Au clusters on semiconductor surfaces can serve as epoxidation catalysts for these alkenes [5,29]. Here, we report on the interactions of Ag_m^+ ($m=3-13$) with C_2H_4 and on the interactions of Ag_m^+ ($m=3-9$) with C_3H_6 obtained from temperature-dependent equilibrium methods and ab initio calculations.

2. Experimental methods

A description of the instrument and experimental details has been given previously [12,13,30], and only a brief description will be given here. Silver ions are generated by pulsed laser vaporization of a translating/rotating silver rod in a high-pressure Ar bath gas. Silver clusters exiting the source are then mass selected by a quadrupole mass filter and injected into a 4 cm long drift/reaction cell containing a mixture of reactant gas (either C_2H_4 or C_3H_6) and He. The typical composition of the gas mixture is 4.5 Torr of He combined with 0.01 to 0.5 Torr of either C_2H_4 or C_3H_6 . Equilibria (Eq. (1) where either $m=3-13$ and

* Corresponding author. Tel.: +1 805 893 2893; fax: +1 805 893 8703.
E-mail address: bowers@chem.ucsb.edu (M.T. Bowers).

$L = C_2H_4$ or $m = 3-9$ and $L = C_3H_6$) are quickly established as the various silver–alkene clusters are drawn through the cell under the influence of a small electric field.



The electric field is small enough so that the thermal energy of the ions is not significantly perturbed. The clusters exiting the cell are then mass selected by a second quadrupole and detected.

Integrated peak areas are recorded and these values, along with the pressure of the ligating gas (P_L) in Torr, are used to determine an equilibrium constant (K_P°) for each reaction using Eq. (2).

$$K_P^\circ = \frac{[Ag_m^+(L)_n]}{[Ag_m^+(L)_{n-1}]} \times \frac{760}{P_L} \quad (2)$$

The equilibrium constants can then be used to calculate the standard Gibbs free energies for the reactions,

$$\Delta G_T^\circ = -RT \ln(K_P^\circ) \quad (3)$$

and the values obtained for ΔG_T° plotted versus the temperature, to obtain ΔS_T° and ΔH_T° for each reaction using Eq. (4).

$$\Delta G_T^\circ = \Delta H_T^\circ - T \Delta S_T^\circ \quad (4)$$

The resulting plots are linear over the experimental temperature range for all systems reported here. A least squares fitting procedure is used to obtain the slope and intercept of each line. The slopes determine the association entropy for Eq. (1) (ΔS_T°) and the intercepts give the corresponding ΔH_T° values. The reported uncertainty in these values is a measure of variance in the data from the fit. The 0 K bond dissociation energy (BDE) is then determined by fitting and extrapolating the data to 0 K using statistical thermodynamics. The necessary vibrational frequencies and rotational constants are taken from density functional theory (DFT) [31] calculations (see Section 3). In all cases, vibrational frequencies are varied over a wide range of physically reasonable values, and the effect on ΔH_0° is included in the error limits. It should be stressed that uncertainties in these parameters have little effect on the final values of ΔH_0° . A thorough discussion of this fitting procedure and an estimation of the errors involved has been given previously [30,32].

3. Theory

The product ions of interest were examined theoretically to determine the molecular parameters needed to analyze the experimental data and to identify factors important in the bonding, including 0 K BDE's (D_0) for comparison with the experimentally determined values ($-\Delta H_0^\circ$). DFT calculations were carried out using the B3LYP hybrid functional [33,34] and the Gaussian 03 package [35]. For all of the calculations reported here, carbon and hydrogen were described using the standard 6-31+G** basis set [36]. The basis set for silver is a (5s6p4d)/[3s3p2d] contraction of the Hay–Wadt ($n+1$) effective core potential (ECP) valence double zeta basis proposed by Hay and Wadt [37,38]. Here, the outermost core orbitals are not replaced by the ECP, but

are instead treated equally with the valence orbitals. This allows for increased accuracy in the calculations without a substantial increase in computation time. The ECP for silver incorporates the Darwin and mass–velocity relativistic effects into the potential.

Geometry optimizations of $Ag_m^+(C_2H_4)_n$ and $Ag_m^+(C_3H_6)_n$ clusters of interest were performed over a wide variety of conceivable geometries in order to obtain minimum energy cluster conformations and to ensure that no alternate theoretical geometries exist that significantly differ from those reported here. All confirmed minima consist of largely unperturbed C_2H_4 and C_3H_6 ligands bound to a metal core ion.

4. Results

Plots of ΔG_T° versus T for the additions of C_2H_4 and C_3H_6 to Ag_4^+ are given in Fig. 1 and similar plots for C_2H_4 and

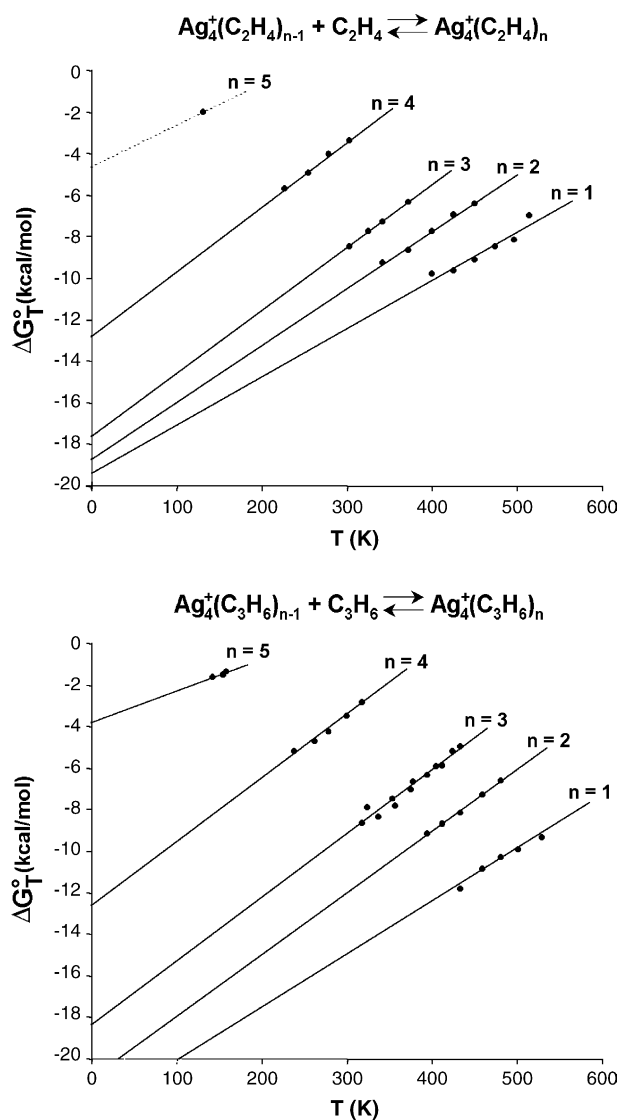


Fig. 1. Plot of experimental ΔG_T° vs. temperature data for the association reactions $Ag_4^+(L)_{n-1} + L \rightleftharpoons Ag_4^+(L)_n$ (L is either C_2H_4 or C_3H_6). For $n=5$ of the C_2H_4 system, the slope of the line is 10 cal/(mol K) more positive than the $n=4$ line (see text for details).

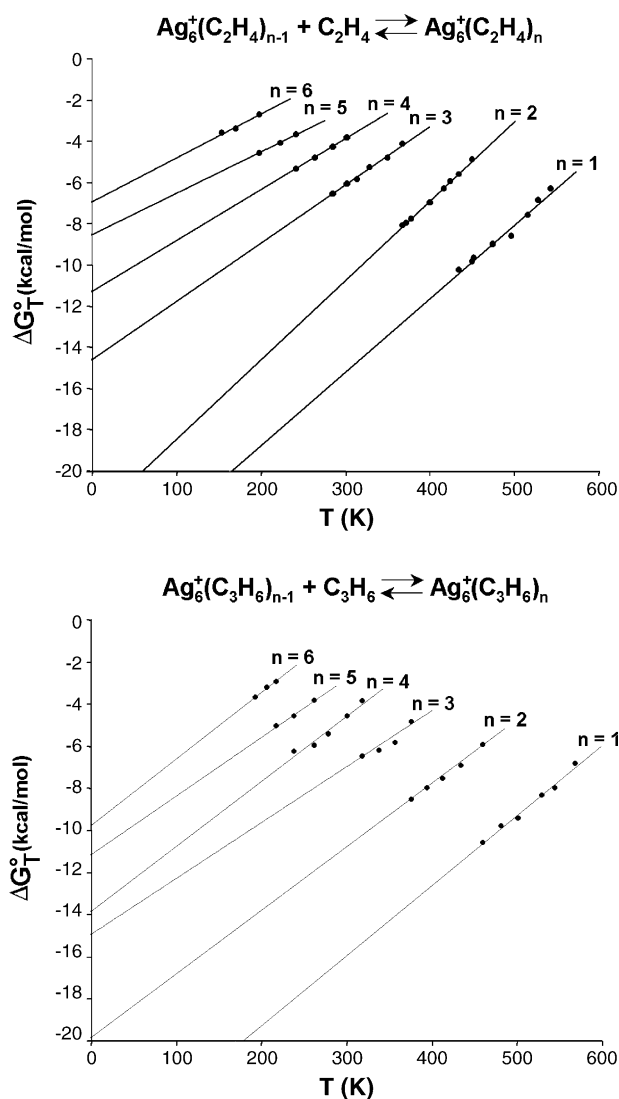


Fig. 2. Plot of experimental ΔG_T^0 vs. temperature data for the association reactions $\text{Ag}_4^+(\text{L})_{n-1} + \text{L} \rightleftharpoons \text{Ag}_4^+(\text{L})_n$ (L = either C_2H_4 or C_3H_6).

C_3H_6 additions to Ag_6^+ are given in Fig. 2. All other ΔG_T^0 versus T data plots for the systems discussed here can either be found in supplementary information or have been published elsewhere [28]. The intercepts and slopes of the lines yield the ΔH_T^0 and ΔS_T^0 values given in Tables 1–11 for the $\text{Ag}_m^+(\text{C}_2\text{H}_4)_n$ ($m=3$ –13) systems, respectively, and in Tables 12–18 for the

Table 1
Data summary for $\text{Ag}_3^+(\text{C}_2\text{H}_4)_{n-1} + \text{C}_2\text{H}_4 \rightleftharpoons \text{Ag}_3^+(\text{C}_2\text{H}_4)_n$

n	Experiment				Theory	
	$-\Delta H_T^0$ ^{a,b}	$-\Delta S_T^0$ ^{a,c}	$-\Delta H_0^0$ ^b	T ^d	D_e ^b	D_0 ^b
1	21.6 ± 0.5	23.1 ± 1	21.5 ± 0.8	450–675	17.84	16.55
2	19.8 ± 0.6	26.0 ± 1	19.7 ± 0.9	375–575	15.23	14.15
3	17.3 ± 0.3	28.5 ± 1	17.1 ± 0.6	300–425	12.39	11.17
4	5.7 ± 0.4	19.7 ± 3	5.5 ± 0.6	130–195	–	–

^a Values have been previously reported [28].

^b In units of kcal/mol.

^c In units of cal/(mol K).

^d Temperature range over which equilibrium data was acquired, in Kelvin.

Table 2

Data summary for $\text{Ag}_4^+(\text{C}_2\text{H}_4)_{n-1} + \text{C}_2\text{H}_4 \rightleftharpoons \text{Ag}_4^+(\text{C}_2\text{H}_4)_n$

n	Experiment				Theory	
	$-\Delta H_T^0$ ^a	$-\Delta S_T^0$ ^b	$-\Delta H_0^0$ ^a	T ^c	D_e ^a	D_0 ^a
1	19.4 ± 1.4	23.3 ± 4	19.2 ± 1.8	400–515	16.15	14.80
2	18.7 ± 0.6	27.4 ± 2	18.6 ± 0.9	340–450	12.53	11.53
3	17.6 ± 0.2	30.2 ± 1	17.4 ± 0.5	300–375	10.18	9.11
4	12.8 ± 0.5	31.1 ± 2	12.5 ± 0.7	225–300	7.52	6.60
5	–	–	~ 4.6 ^d	130	–	–

^a In units of kcal/mol.

^b In units of cal/(mol K).

^c Temperature range over which equilibrium data was acquired, in Kelvin.

^d Estimated by assuming that the association entropy was 10 cal/(mol K) more positive than that of the previous ligand addition.

Table 3

Data summary for $\text{Ag}_5^+(\text{C}_2\text{H}_4)_{n-1} + \text{C}_2\text{H}_4 \rightleftharpoons \text{Ag}_5^+(\text{C}_2\text{H}_4)_n$

n	Experiment				Theory	
	$-\Delta H_T^0$ ^{a,b}	$-\Delta S_T^0$ ^{a,c}	$-\Delta H_0^0$ ^b	T ^d	D_e ^b	D_0 ^b
1	18.8 ± 0.8	24.3 ± 2	18.7 ± 1.1	400–535	13.88	12.73
2	18.4 ± 0.8	27.8 ± 2	18.2 ± 1.2	375–455	12.23	11.07
3	25.9 ± 0.5	45.3 ± 1	25.2 ± 0.9	370–435	10.77	8.93
4	9.3 ± 0.4	23.3 ± 2	8.9 ± 0.6	195–265	4.37	3.58
5	6.9 ± 0.4	21.1 ± 2	6.7 ± 0.6	155–200	2.69	2.07
6	4.5 ± 0.4	12.6 ± 2	4.5 ± 0.6	130–170	–	–

^a Values have been previously reported [28].

^b In units of kcal/mol.

^c In units of cal/(mol K).

^d Temperature range over which equilibrium data was acquired, in Kelvin.

Table 4

Data summary for $\text{Ag}_6^+(\text{C}_2\text{H}_4)_{n-1} + \text{C}_2\text{H}_4 \rightleftharpoons \text{Ag}_6^+(\text{C}_2\text{H}_4)_n$

n	Experiment				Theory	
	$-\Delta H_T^0$ ^a	$-\Delta S_T^0$ ^b	$-\Delta H_0^0$ ^a	T ^c	D_e ^a	D_0 ^a
1	26.0 ± 0.8	35.8 ± 2	25.7 ± 1.0	435–545	17.18	15.77
2	22.3 ± 0.3	38.5 ± 1	22.0 ± 0.6	370–455	13.50	12.20
3	14.8 ± 0.4	28.8 ± 1	14.6 ± 0.7	285–370	8.48	7.53
4	11.4 ± 0.3	25.1 ± 1	11.2 ± 0.6	245–300	6.48	5.53
5	8.6 ± 0.4	20.3 ± 2	8.5 ± 0.6	200–245	4.19	3.51
6	6.9 ± 0.6	20.7 ± 3	6.9 ± 0.8	155–200	3.22	2.52

^a In units of kcal/mol.

^b In units of cal/(mol K).

^c Temperature range over which equilibrium data was acquired, in Kelvin.

Table 5

Data summary for $\text{Ag}_7^+(\text{C}_2\text{H}_4)_{n-1} + \text{C}_2\text{H}_4 \rightleftharpoons \text{Ag}_7^+(\text{C}_2\text{H}_4)_n$

n	Experiment				Theory	
	$-\Delta H_T^0$ ^a	$-\Delta S_T^0$ ^b	$-\Delta H_0^0$ ^a	T ^c	D_e ^a	D_0 ^a
1	26.7 ± 0.5	38.7 ± 1	26.4 ± 0.7	435–545	16.54	15.14
2	22.5 ± 0.7	36.6 ± 2	22.1 ± 1.0	370–455	14.09	12.78
3	12.9 ± 0.3	26.3 ± 1	12.7 ± 0.6	265–330	7.23	6.26
4	10.1 ± 0.2	21.3 ± 1	9.9 ± 0.5	225–300	6.55	5.64
5	8.2 ± 0.4	18.6 ± 2	7.9 ± 0.7	200–245	4.84	3.98
6	6.5 ± 0.5	16.9 ± 3	6.3 ± 0.7	155–200	2.99	2.35
7	5.6 ± 0.5	18.6 ± 3	5.2 ± 0.8	130–170	1.80	1.20

^a In units of kcal/mol.

^b In units of cal/(mol K).

^c Temperature range over which equilibrium data was acquired, in Kelvin.

Table 6

Data summary for $\text{Ag}_8^+(\text{C}_2\text{H}_4)_{n-1} + \text{C}_2\text{H}_4 \rightleftharpoons \text{Ag}_8^+(\text{C}_2\text{H}_4)_n$

<i>n</i>	Experiment				Theory	
	$-\Delta H_T^{\circ a}$	$-\Delta S_T^{\circ b}$	$-\Delta H_0^{\circ a}$	T^c	D_e^a	D_0^a
1	17.7 ± 0.7	30.0 ± 3	17.5 ± 1.0	330–415	10.96	9.87
2	15.5 ± 0.4	29.5 ± 1	15.3 ± 0.6	285–370	9.78	8.73
3	11.3 ± 0.2	23.1 ± 1	11.0 ± 0.5	245–300	8.49	7.39
4	10.8 ± 0.6	26.4 ± 2	10.5 ± 0.8	225–265	5.68	4.78
5	9.7 ± 0.6	27.3 ± 3	–	200–245	–	–
6	7.2 ± 0.4	20.8 ± 2	–	155–200	–	–
7	6.2 ± 0.6	20.4 ± 3	–	130–170	–	–
8	$\sim 5.6^d$	–	–	130	–	–

^a In units of kcal/mol.^b In units of cal/(mol K).^c Temperature range over which equilibrium data was acquired, in Kelvin.^d Estimate, acquired by assuming the same association entropy as $n=7$.

Table 7

Data summary for $\text{Ag}_9^+(\text{C}_2\text{H}_4)_{n-1} + \text{C}_2\text{H}_4 \rightleftharpoons \text{Ag}_9^+(\text{C}_2\text{H}_4)_n$

<i>n</i>	Experiment				Theory	
	$-\Delta H_T^{\circ a}$	$-\Delta S_T^{\circ b}$	$-\Delta H_0^{\circ a}$	T^c	D_e^a	D_0^a
1	16.5 ± 0.6	26.9 ± 2	16.3 ± 0.8	330–380	9.22	8.15
2	14.9 ± 0.7	29.8 ± 3	14.8 ± 0.9	285–330	8.34	7.43
3	12.7 ± 0.4	28.6 ± 2	12.4 ± 0.7	245–300	7.67	6.61
4	10.8 ± 0.2	27.3 ± 1	10.8 ± 0.5	225–265	3.50	2.88
5	9.6 ± 0.4	27.9 ± 2	9.5 ± 0.7	200–245	3.30	2.62
6	8.1 ± 0.4	25.1 ± 2	–	155–200	–	–
7	6.7 ± 0.4	24.6 ± 2	–	130–170	–	–

^a In units of kcal/mol.^b In units of cal/(mol K).^c Temperature range over which equilibrium data was acquired, in Kelvin.

Table 8

Data summary for $\text{Ag}_{10}^+(\text{C}_2\text{H}_4)_{n-1} + \text{C}_2\text{H}_4 \rightleftharpoons \text{Ag}_{10}^+(\text{C}_2\text{H}_4)_n$

<i>n</i>	Experiment				Theory	
	$-\Delta H_T^{\circ a}$	$-\Delta S_T^{\circ b}$	$-\Delta H_0^{\circ a}$	T^c	D_e^a	D_0^a
1	14.8 ± 0.7	25.8 ± 2	14.7 ± 0.9	305–375	7.43	6.44
2	15.9 ± 0.5	30.7 ± 2	15.7 ± 0.7	305–375	9.79	8.74

^a In units of kcal/mol.^b In units of cal/(mol K).^c Temperature range over which equilibrium data was acquired, in Kelvin.

Table 9

Data summary for $\text{Ag}_{11}^+(\text{C}_2\text{H}_4)_{n-1} + \text{C}_2\text{H}_4 \rightleftharpoons \text{Ag}_{11}^+(\text{C}_2\text{H}_4)_n$

<i>n</i>	Experiment				Theory	
	$-\Delta H_T^{\circ a}$	$-\Delta S_T^{\circ b}$	$-\Delta H_0^{\circ a}$	T^c	D_e^a	D_0^a
1	$14.8 \pm 0.528.5 \pm 1$		14.7 ± 0.7	305–390	7.97	6.86
2	$13.8 \pm 0.826.9 \pm 3$		13.7 ± 1.0	290–350	7.30	6.41

^a In units of kcal/mol.^b In units of cal/(mol K).^c Temperature range over which equilibrium data was acquired, in Kelvin.

Table 10

Data summary for $\text{Ag}_{12}^+(\text{C}_2\text{H}_4)_{n-1} + \text{C}_2\text{H}_4 \rightleftharpoons \text{Ag}_{12}^+(\text{C}_2\text{H}_4)_n$

<i>n</i>	Experiment				Theory	
	$-\Delta H_T^{\circ a}$	$-\Delta S_T^{\circ b}$	$-\Delta H_0^{\circ a}$	T^c	D_e^a	D_0^a
1	16.7 ± 0.6	31.3 ± 2	16.5 ± 0.8	290–390	9.71	8.67
2	13.6 ± 0.7	25.7 ± 2	13.4 ± 0.9	280–390	8.72	7.69

^a In units of kcal/mol.^b In units of cal/(mol K).^c Temperature range over which equilibrium data was acquired, in Kelvin.

Table 11

Data summary for $\text{Ag}_{13}^+(\text{C}_2\text{H}_4)_{n-1} + \text{C}_2\text{H}_4 \rightleftharpoons \text{Ag}_{13}^+(\text{C}_2\text{H}_4)_n$

<i>n</i>	Experiment				Theory	
	$-\Delta H_T^{\circ a}$	$-\Delta S_T^{\circ b}$	$-\Delta H_0^{\circ a}$	T^c	D_e^a	D_0^a
1	16.3 ± 0.4	32.3 ± 1	16.2 ± 0.6	290–390	7.94	6.96

^a In units of kcal/mol.^b In units of cal/(mol K).^c Temperature range over which equilibrium data was acquired, in Kelvin.

Table 12

Data summary for $\text{Ag}_3^+(\text{C}_3\text{H}_6)_{n-1} + \text{C}_3\text{H}_6 \rightleftharpoons \text{Ag}_3^+(\text{C}_3\text{H}_6)_n$

<i>n</i>	Experiment				Theory	
	$-\Delta H_T^{\circ a}$	$-\Delta S_T^{\circ b}$	$-\Delta H_0^{\circ a}$	T^c	D_e^a	D_0^a
1	26.2 ± 0.6	27.5 ± 2	26.1 ± 1.0	555–745	19.51	18.46
2	21.4 ± 0.9	26.4 ± 2	21.3 ± 1.5	465–570	16.12	15.21
3	18.9 ± 0.4	31.1 ± 1	18.7 ± 0.9	355–465	12.76	11.88
4	4.9 ± 0.2	15.0 ± 1	4.9 ± 0.4	145–280	–	–
5	4.3 ± 0.6	18.1 ± 3	4.2 ± 0.8	175–145	–	–

^a In units of kcal/mol.^b In units of cal/(mol K).^c Temperature range over which equilibrium data was acquired, in Kelvin.

Table 13

Data summary for $\text{Ag}_4^+(\text{C}_3\text{H}_6)_{n-1} + \text{C}_3\text{H}_6 \rightleftharpoons \text{Ag}_4^+(\text{C}_3\text{H}_6)_n$

<i>n</i>	Experiment				Theory	
	$-\Delta H_T^{\circ a}$	$-\Delta S_T^{\circ b}$	$-\Delta H_0^{\circ a}$	T^c	D_e^a	D_0^a
1	22.8 ± 1.1	25.7 ± 3	22.8 ± 1.5	435–530	17.27	16.21
2	21.0 ± 0.5	29.9 ± 1	21.0 ± 0.9	395–480	16.41	15.43
3	18.4 ± 0.7	30.7 ± 2	18.3 ± 1.1	320–435	10.59	9.82
4	12.5 ± 0.6	29.8 ± 2	12.5 ± 0.9	235–325	7.39	6.76
5	3.8 ± 0.6	15.1 ± 3	–	145–160	–	–

^a In units of kcal/mol.^b In units of cal/(mol K).^c Temperature range over which equilibrium data was acquired, in Kelvin.

Table 14

Data summary for $\text{Ag}_5^+(\text{C}_3\text{H}_6)_{n-1} + \text{C}_3\text{H}_6 \rightleftharpoons \text{Ag}_5^+(\text{C}_3\text{H}_6)_n$

<i>n</i>	Experiment				Theory	
	$-\Delta H_T^{\circ a}$	$-\Delta S_T^{\circ b}$	$-\Delta H_0^{\circ a}$	T^c	D_e^a	D_0^a
1	21.7 ± 0.4	27.3 ± 1	21.6 ± 0.7	415–545	14.73	13.78
2	20.5 ± 0.7	29.6 ± 2	19.8 ± 1.0	395–480	13.70	12.65
3	25.3 ± 0.4	44.3 ± 1	25.0 ± 1.0	375–460	8.97	7.56
4	11.3 ± 0.6	28.4 ± 2	11.3 ± 0.9	205–280	4.17	3.63
5	9.4 ± 0.7	30.6 ± 3	9.4 ± 1.0	190–220	2.11	1.73
6	6.0 ± 0.7	21.4 ± 3	–	145–170	–	–

^a In units of kcal/mol.^b In units of cal/(mol K).^c Temperature range over which equilibrium data was acquired, in Kelvin.

Table 15

Data summary for $\text{Ag}_6^+(\text{C}_3\text{H}_6)_{n-1} + \text{C}_3\text{H}_6 \rightleftharpoons \text{Ag}_6^+(\text{C}_3\text{H}_6)_n$

<i>n</i>	Experiment				Theory	
	$-\Delta H_T^\circ{}^a$	$-\Delta S_T^\circ{}^b$	$-\Delta H_0^\circ{}^a$	T^c	D_e^a	D_0^a
1	25.9 ± 0.9	33.3 ± 2	25.8 ± 1.2	460–570	17.78	16.57
2	20.0 ± 0.7	30.3 ± 2	19.8 ± 1.1	375–460	13.65	12.64
3	15.0 ± 1.0	26.5 ± 3	14.9 ± 1.4	300–375	8.31	7.49
4	13.9 ± 1.1	30.9 ± 3	13.9 ± 1.4	240–320	6.18	5.42
5	11.1 ± 0.6	27.8 ± 2	–	220–260	–	–
6	9.8 ± 0.5	31.5 ± 2	–	190–220	–	–

^a In units of kcal/mol.^b In units of cal/(mol K).^c Temperature range over which equilibrium data was acquired, in Kelvin.

Table 16

Data summary for $\text{Ag}_7^+(\text{C}_3\text{H}_6)_{n-1} + \text{C}_3\text{H}_6 \rightleftharpoons \text{Ag}_7^+(\text{C}_3\text{H}_6)_n$

<i>n</i>	Experiment				Theory	
	$-\Delta H_T^\circ{}^a$	$-\Delta S_T^\circ{}^b$	$-\Delta H_0^\circ{}^a$	T^c	D_e^a	D_0^a
1	25.2 ± 1.0	33.4 ± 2	25.1 ± 1.3	460–570	16.87	15.75
2	21.0 ± 0.9	31.5 ± 2	20.8 ± 1.3	375–460	14.07	13.00
3	14.4 ± 0.5	27.2 ± 2	14.3 ± 0.9	280–375	7.30	6.52
4	13.2 ± 0.8	29.2 ± 3	13.1 ± 1.1	240–300	5.93	5.14
5	12.0 ± 0.3	30.8 ± 1	–	220–260	–	–
6	10.8 ± 0.3	32.7 ± 1	–	190–220	–	–
7	8.5 ± 0.2	30.5 ± 1	–	155–190	–	–

^a In units of kcal/mol.^b In units of cal/(mol K).^c Temperature range over which equilibrium data was acquired, in Kelvin.

$\text{Ag}_m^+(\text{C}_3\text{H}_6)_n$ ($m=3-9$) systems, respectively. ΔH_0° values obtained as previously described are also listed in Tables 1–18 for each silver–alkene system examined.

Several trends in the experimental data were observed. With the exception of Ag_5^+ and Ag_{10}^+ , the strongest silver–alkene bond results from the addition of the first ligand to the transition metal core ion, although the decrease in the binding energies of successive ligand additions vary substantially and are unique to each silver cluster. The BDEs of the $\text{Ag}_m^+/\text{C}_3\text{H}_6$ system are systematically larger than those of the $\text{Ag}_m^+/\text{C}_2\text{H}_4$ system for a given value of m .

Trends in the association entropies for the systems studied can also be seen. Typical ΔS_T° values ranged from approximately -20 cal/(mol K) to -30 cal/(mol K). All association reactions

Table 17

Data summary for $\text{Ag}_8^+(\text{C}_3\text{H}_6)_{n-1} + \text{C}_3\text{H}_6 \rightleftharpoons \text{Ag}_8^+(\text{C}_3\text{H}_6)_n$

<i>n</i>	Experiment				Theory	
	$-\Delta H_T^\circ{}^a$	$-\Delta S_T^\circ{}^b$	$-\Delta H_0^\circ{}^a$	T^c	D_e^a	D_0^a
1	19.7 ± 0.8	29.9 ± 2	19.7 ± 1.0	375–460	12.07	11.15
2	16.9 ± 0.5	29.5 ± 1	16.9 ± 0.8	320–400	10.49	9.58
3	15.2 ± 0.3	32.6 ± 1	15.2 ± 0.6	280–320	6.61	5.85
4	12.9 ± 0.6	30.6 ± 2	–	240–280	–	–
5	11.6 ± 0.3	31.3 ± 1	–	205–240	–	–
6	10.6 ± 0.5	32.6 ± 2	–	190–220	–	–
7	$\sim 8.3^d$	$\sim 31.0^d$	–	155–170	–	–

^a In units of kcal/mol.^b In units of cal/(mol K).^c Temperature range over which equilibrium data was acquired, in Kelvin.^d Estimate, values obtained from two data points.

Table 18

Data summary for $\text{Ag}_9^+(\text{C}_3\text{H}_6)_{n-1} + \text{C}_3\text{H}_6 \rightleftharpoons \text{Ag}_9^+(\text{C}_3\text{H}_6)_n$

<i>n</i>	Experiment				Theory	
	$-\Delta H_T^\circ{}^a$	$-\Delta S_T^\circ{}^b$	$-\Delta H_0^\circ{}^a$	T^c	D_e^a	D_0^a
1	19.3 ± 0.6	29.6 ± 2	19.2 ± 0.8	375–460	10.12	9.30
2	16.2 ± 0.5	28.7 ± 2	16.2 ± 0.7	320–375	9.09	8.28
3	14.6 ± 0.8	30.7 ± 3	14.5 ± 1.1	280–320	7.95	7.19
4	13.0 ± 0.8	31.2 ± 3	–	240–280	–	–
5	11.2 ± 0.4	30.6 ± 2	–	205–240	–	–
6	10.2 ± 0.2	32.6 ± 1	–	190–220	–	–
7	8.5 ± 0.2	28.9 ± 1	–	155–190	–	–
8	$\sim 7.0^d$	$\sim 28.5^d$	–	140–155	–	–

^a In units of kcal/mol.^b In units of cal/(mol K).^c Temperature range over which equilibrium data was acquired, in Kelvin.^d Estimate, values obtained from two data points.

(Eq. (1)) where the value of $n > m$ result in values of ΔS_T° that are approximately 10 entropy units “less negative” than those of the first m ligands. Some association reactions give rise to values of ΔS_T° that are much more negative than -30 cal/(mol K). The reasons for these large negative values of ΔS_T° are unique to the system in which it occurs and each case will be discussed in detail in the following sections.

A trend concerning the BDEs of the first alkene ligand additions to the Ag_m^+ clusters is also observed. With the exception

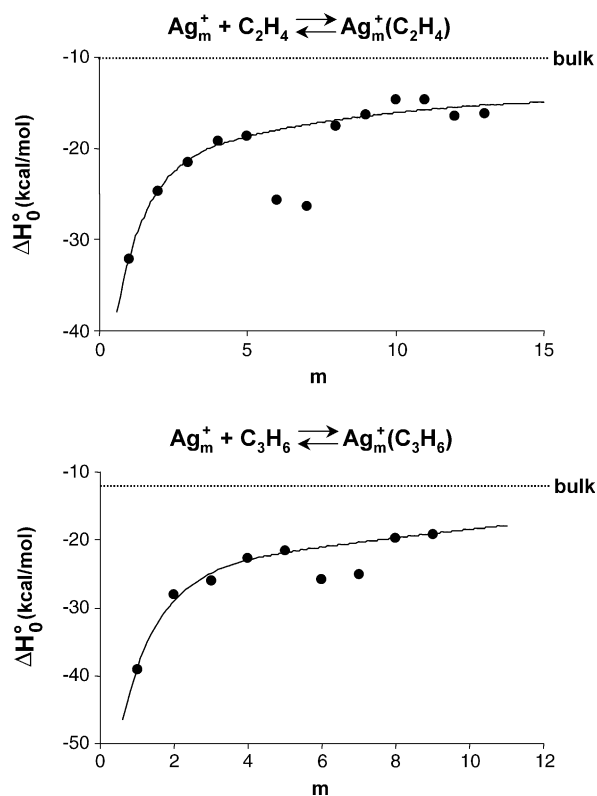


Fig. 3. Plot of ΔH_0° vs. cluster size (m) for the association reactions $\text{Ag}_m^+ + \text{L} \rightleftharpoons \text{Ag}_m^+(\text{L})$ ($m=3-13$, $\text{L}=\text{C}_2\text{H}_4$; $m=3-9$, $\text{L}=\text{C}_3\text{H}_6$). The curve through the data points is provided to guide the eye. Dashed lines indicate the binding energy of the respective alkene ligands to an $\text{Ag}(110)$ surface.

of the Ag_6^+ and Ag_7^+ clusters, the BDEs of the first alkene ligands systematically decrease as the size of the Ag_m^+ clusters increase, as shown in Fig. 3. Fig. 3 also shows that the BDEs appear to be asymptotically approaching the binding energy of C_2H_4 and C_3H_6 to the bulk silver surface.

The energies and geometries of ligated silver cluster ions were calculated using DFT. Ethene and propene ligand binding energies obtained from these calculations are given in Tables 1–18 for comparison with the corresponding experimental BDEs. DFT calculations provide binding energies in good quantitative agreement with experiment for the early ligand additions to the smaller Ag_m^+ ($m = 3–5$) clusters. The quantitative agreement worsens for the larger clusters with more ligands attached, but the experimental trends in binding energies are nicely duplicated. The geometries of $\text{Ag}_4^+(\text{C}_2\text{H}_4)_{1–5}$, $\text{Ag}_4^+(\text{C}_3\text{H}_6)_{1–5}$ and $\text{Ag}_6^+(\text{C}_2\text{H}_4)_{1–6}$, are published here as examples of ligated structures (Figs. 4 and 5). The DFT structures for all other clusters involved in Eq. (1) are available upon request. Theoretical molecular geometries and electronic population analysis provided information necessary to identify factors important in the binding interactions of the various clusters.

5. Discussion


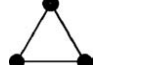

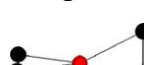


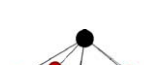



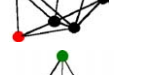

5.1. Binding interactions of silver–alkene clusters

A detailed understanding of the interactions between the silver cluster ions and their alkene ligands can be achieved by examining the valence electronic configurations of each species separately. Recently, Weis et al. used ion mobility spectrometry along with DFT to investigate bare silver cluster cations [39]. Using this combination of theory and experiment, they were able to determine cluster geometries. We have used their results as a basis for our own DFT calculations to determine natural bond order (NBO) populations [40]. These results are given in Table 19 along with the bare silver cluster geometries. NBO analysis shows that the highest occupied molecular orbitals (HOMO) of the Ag_m^+ clusters are created by overlap of the 5s orbitals of each Ag atom in a given cluster. For each Ag_m^+ cluster, one of these 5s orbitals is initially unoccupied, giving rise to the positive charge of the cluster. The remaining ($m - 1$) 5s orbitals are singly occupied. In most cases the electron density is delocalized about the cluster. Equivalent amounts of electron density located on two or more atoms of a cluster (see Table 19) are found for metal clusters having highly symmetric geometries. To understand the binding interactions of a silver–alkene cluster we must also consider the valence electronic configurations of C_2H_4 and C_3H_6 . These species are well characterized. The HOMOs of C_2H_4 and C_3H_6 are the $\pi(2p_y)^2$ bonding orbitals that makes up the C–C double bond in both molecules.

A series of DFT calculations performed by Chretien et al. [41] indicate that absorption of an electron donating ligand to a coinage metal cluster preferentially occurs at the location where the lowest unoccupied molecular orbital (LUMO) of the metal clusters protrudes most into the vacuum. This location is found on atoms located at “corners” of the metal clusters.

Table 19

Natural bond order populations and charges of the Ag_m^+ clusters ($m = 2–13$)

m	Structure ^a	Symmetry	5s populations ^b	5s charges ^b
2		$D_{\infty h}$	0.500	0.500
3		D_{3h}	0.666	0.333
4		D_{2h}	0.722 0.759	0.254 0.245
5		D_{2d}	0.744 1.005	0.258 -0.030
6		C_{2v}	0.585 0.899 0.952	0.354 0.091 0.056
7		D_{5h}	0.522 0.953	0.378 0.049
8 ^c		C_s	0.823	0.184
9		D_{3h}	0.856 0.876	0.137 0.098
10		C_s	0.857 0.953	0.113 0.048
11		D_{3h}	0.807 0.906 1.060	0.136 0.093 -0.047
12 ^c		C_{2v}	0.844	0.130
13 ^c		C_{2v}	0.823	0.121

For interpretation of the references to color in this table, the reader is referred to the web version of this article.

^a Cluster geometries obtained from ion mobility data [39] and DFT calculations. Ag atoms of a given cluster having equal charge distributions are identically colored.

^b Populations for the 5s atomic orbitals of the Ag atoms of each cluster and the corresponding partial atomic charge. Text color corresponds to analogously colored atoms of a given structure.

^c Only populations and charges of atoms having the greatest amount of partial positive charge (shown in black) are given for these clusters.

Additionally, for the entire series of positively charged cluster ions studied here, our DFT calculations indicate that the position of the LUMO directly correlates with the location of highest partial-positive charge of a cluster. This implies that alkene lig-

and additions to the Ag_m^+ clusters occur at the Ag atom carrying the most partial-positive charge.

NBO analysis shows that for the addition of the first m ligands to the Ag_m^+ clusters, a substantial amount of electron density is transferred from the ligand to the transition metal cluster. The exact amount of electron density donated varies with cluster size and with the alkene ligand (either C_2H_4 or C_3H_6). This electron density originates from the $\pi(2p_y)^2$ bonding orbitals of C_2H_4 and C_3H_6 and is donated to the LUMO of the Ag_m^+ clusters. This type of donation is consistent with what has been previously reported for the interactions of C_2H_4 and C_3H_6 with $\text{Ag}_{1,2}^+$ [27] and suggests that the primary silver–alkene binding interaction continues to be covalent in nature for the larger silver clusters.

The interaction of C_3H_6 with the Ag_m^+ clusters is systematically stronger than that of C_2H_4 . NBO shows that electron donation from C_3H_6 to the Ag_m^+ clusters is slightly larger than for C_2H_4 for a given value of m . This result suggests the larger BDEs of the silver–propene clusters are a result of a slightly stronger covalent interaction. However, it should also be noted that C_3H_6 has both a larger polarizability than C_2H_4 (6.3 \AA^3 versus 4.3 \AA^3) [42] and dipole moment (0.44 D versus 0.0 D

according to DFT) indicating electrostatic forces could also contribute to the differences in the observed binding energies.

From the theoretical silver–alkene molecular geometries given in Figs. 4 and 5, it is apparent that both types of alkene ligands adsorb side-on to the Ag_m^+ clusters, perpendicular to the silver–alkene bond axis. This orientation allows for optimum molecular orbital overlap between the Ag_m^+ clusters and the alkene ligands. Additionally, the calculated C–C double bond distances for ligands of an $\text{Ag}_m^+(\text{L})_n$ cluster, where $n \leq m$, are increased slightly compared to that of free the molecules, consistent with electron transfer out of a bonding orbital.

5.2. Sequential ligand additions to individual Ag_m^+ clusters

Plots of ΔG_T° versus T provide information as to the manner in which sequential C_2H_4 and C_3H_6 additions to the Ag_m^+ clusters occur. Plots were generated for each system described by Eq. (1) and were found to fall into one of two groups. The first group accounts for ligand additions to a silver cluster in which all for the atoms of the cluster have equal or nearly equal charge distributions. For the purposes of this discussion, the Ag_4^+

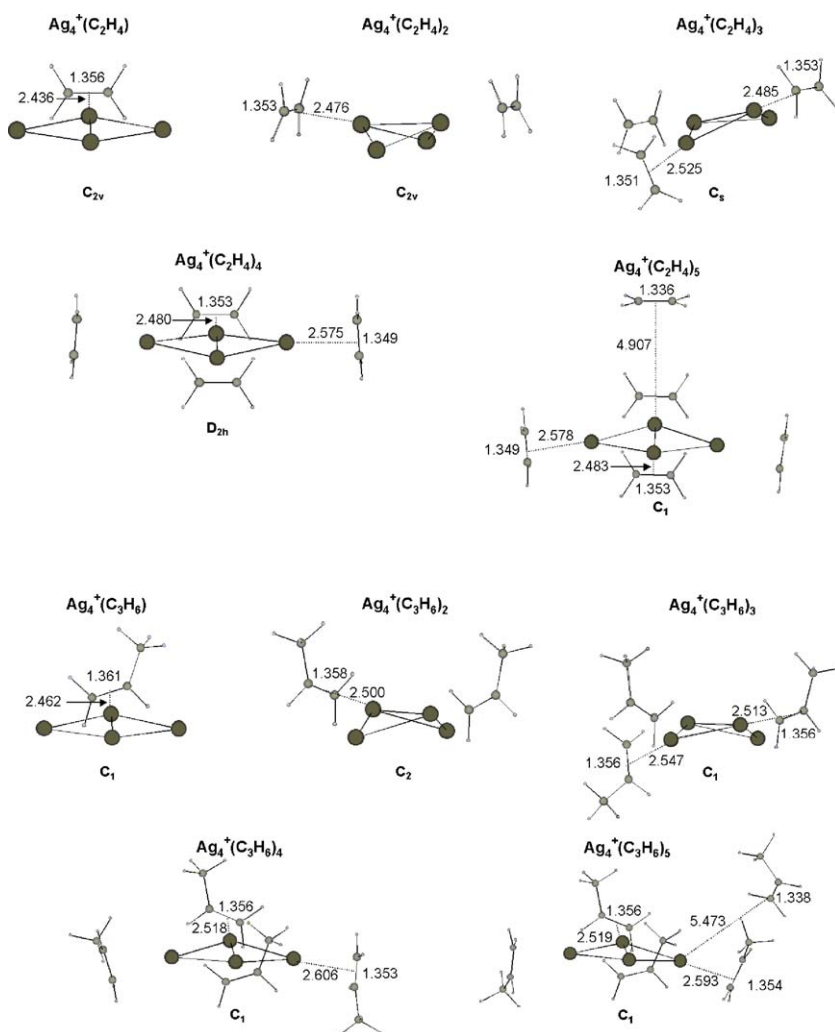


Fig. 4. Theoretical geometries of the $\text{Ag}_4^+(\text{L})_n$ clusters (L = either C_2H_4 or C_3H_6) calculated at the DFT B3LYP level. Distances are in angstroms. All $\text{Ag}_4^+ - \text{L}$ bond distances are measured from the bonding atom of the Ag_4^+ ion to the center of the C–C double bond.

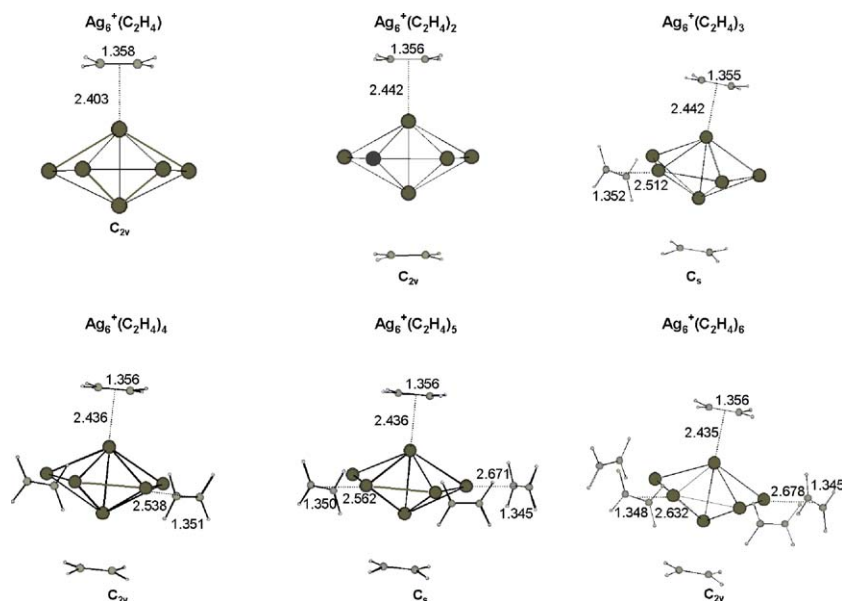


Fig. 5. Theoretical geometries of the $\text{Ag}_6^+(\text{C}_2\text{H}_4)_n$ clusters calculated at the DFT B3LYP level. Distances are in angstroms. All $\text{Ag}_6^+-\text{C}_2\text{H}_4$ bond distances are measured from the bonding atom of the Ag_6^+ ion to the center of the C–C double bond. C_3H_6 additions to Ag_6^+ are analogous to the C_2H_4 system.

cluster will serve as the example for these types of systems. The second group accounts for ligand additions to a silver cluster in which the charge is unequally distributed about the atoms of the metal cluster. The Ag_6^+ cluster will serve as the example for these types of systems.

5.3. Equal Ag_m^+ charge distributions

Five ligand additions are observed for the Ag_4^+ system (Fig. 4). The first four additions have similar BDEs and association entropies (Tables 2 and 13). However, the BDEs do slightly decrease as the number of ligands bound to the cluster increase. The fifth ligand BDE is significantly smaller than the first four. From the structure of Ag_4^+ and the partial atom charges shown in Table 19, it is clear that Ag_4^+ has four nearly electronically equivalent corners. The first four ligands bind to individual corners of the Ag_4^+ cluster until none remain. Since the four corners of Ag_4^+ have similar partial-positive charges, each ligand donates similar amounts of electron density to the transition metal cluster, although the amount does slightly decrease as the number of ligands bound to the metal cluster increases. This decrease is due to increased Pauli repulsion caused by the increase in the amount of electron density present on the metal cluster and can be observed experimentally by small decreases in the BDEs of the $\text{Ag}_4^+(\text{L})_n$ systems as n goes from 1 to 4.

A slightly larger reduction in the BDE of the fourth alkene ligand addition to Ag_4^+ relative to the initial three is observed. This indicates that the $\text{Ag}_4^+(\text{L})_3$ clusters may be an unusually stable structures. The theoretical geometries given in Fig. 4 show that the Ag_4^+ core ion takes on a slightly bent conformation when the second ligand binds and remains that way until addition of a fourth ligand when the metal cluster returns to the original planar geometry. DFT indicates that an alterna-

tive $\text{Ag}_4^+(\text{L})_3$ conformer exists that is energetically degenerate with the structure shown in Fig. 4 in which the Ag_4^+ core forms a quasi-tetrahedral structure with three ligands bound. The tetrahedral geometry of Ag_4^+ is only found to be stable when three ligands are attached and spontaneously reverts back to the structure of $\text{Ag}_4^+(\text{L})_4$ shown in Fig. 4 when the fourth ligand adds. The increased stability of the tetrahedral geometry of Ag_4^+ when three ligands are bound may cause the addition of the fourth ligand to be energetically less favorable than would be the case if the Ag_4^+ core remained in a quasi-planar conformation.

The data for the fifth ligand addition to Ag_4^+ could only be taken over a limited temperature range for the C_3H_6 system (145–160 K) and for the C_2H_4 system only a single data point could be obtained. For all association reactions in which $n > m$ (Eq. (1)), an increase in association entropy occurs by approximately 10 cal/(mol K) relative to the $n = m$ association reaction. This increase indicates that the terminal ligand is much more mobile than the previous additions and hence occupies the second solvation shell. Since all the coordination sites on the metal cluster are occupied, the ligand is essentially unbound and orbiting the $\text{Ag}_m^+(\text{L})_n$ ($n = m$) core ion. DFT calculations are consistent with this observation. All of the calculated binding energies for association reaction in which $n > m$ (Eq. (1)) are approximately 0 kcal/mol, indicating that the ligand is essentially unbound. This is not an uncommon DFT result for ligand addition in the second solvation shell. Theoretical $\text{Ag}_m^+-\text{alkene}$ bond distances for ligand additions in the second solvation shell are generally greater than 5 Å, while the bond distances of the other alkene ligands to the Ag_m^+ cluster remain nearly unchanged (see the $\text{Ag}_4^+(\text{L})_5$ clusters in Fig. 4). The C–C double bond distance of the alkene ligands in the second solvation shell are approximately the same as that calculated for either a free C_2H_4 or C_3H_6 molecule.

5.4. Unequal Ag_m^+ charge distributions

The geometry and valence electron density of bare Ag_6^+ is given in Table 19. Six ligand additions are observed for the Ag_6^+ system (Fig. 5). The first two ligand additions to Ag_6^+ are very strongly bound (Tables 4 and 15). The association entropies, especially for the C_2H_4 system, are also outside the range of typical silver–alkene ligand additions (-20 cal/(mol K) to -30 cal/(mol K)). The reasons for the large BDEs and association entropies of these additions will be discussed in a subsequent section. The BDEs of the next four ligands additions to Ag_6^+ are significantly reduced compared to the initial two. However, the third and the fourth ligands add with similar BDEs, as do the fifth and sixth ligands. In essence, the six alkene ligands bind to Ag_6^+ in a “pairwise” manner.

NBO analysis indicates that there is a large amount of positive charge located on the atoms of Ag_6^+ where the first two ligands bind. This allows the two ligands to donate relatively large amounts of electron density to the metal cluster. There is a large drop in the amount of positive charge located on the four remaining Ag atoms of the cluster. This gives rise to the reduced BDEs of the final four ligand additions to Ag_6^+ . These ligands bind to the cluster in a region of relatively high electron density and the increased Pauli repulsion results in a reduction in the covalent interactions of the ligands with Ag_6^+ . However, the positive charge found in this region is also unequally distributed, with the Ag atoms where the third and fourth ligands bind being slightly more positively charged than Ag atoms where the fifth and sixth ligands add to the cluster. We believe this pairwise distribution of charge is responsible for the manner in which alkene ligands add to Ag_6^+ .

5.5. $\text{Ag}_5^+(\text{L})_3$

The Ag_5^+ system has been discussed previously [28] and therefore will only be briefly mentioned here. It is clear from the BDEs and association entropies given in Tables 3 and 14 that the third alkene ligand addition to Ag_5^+ is unique. The value of ΔS_T° (approximately -45 cal/(mol K)) is much more negative than what is measured for a typical silver–alkene association reaction. The BDE of the third ligand addition to Ag_5^+ is also substantially larger than the previous additions to the cluster.

These phenomena are a result of a ligation-induced conformational change of Ag_5^+ that occurs when the third ligand binds. DFT indicates that the D_{3h} conformation of Ag_5^+ , initially 17.50 kcal/mol higher in energy than the D_{2d} conformer [28,39], becomes the minimum energy structure of Ag_5^+ when the third ligand binds (by 1.94 kcal/mol for C_2H_4 and approximately degenerate for C_3H_6). The three atoms of the D_{3h} conformer where the first three ligands bind are equivalent and highly positively charged. The structural rearrangement of Ag_5^+ allows for greatly increased covalent interactions with these three ligands. NBO also indicates that some back-donation from Ag_5^+ to the unoccupied $\pi^*(2p_y)$ orbitals of the alkene ligands takes place. Additionally, calculations show the loss of low frequency vibrational modes that are found for most of the other $\text{Ag}_m^+(\text{L})_n$ clusters indicating tighter, more ordered bonds for $\text{Ag}_5^+(\text{L})_3$.

The strengthening and tightening of all three ligand bonds is believed to be responsible for the highly negative value of ΔS_T° and the large BDE for loss of the third alkene ligand.

5.6. Dependence of ligand bonding interactions on Ag_m^+ cluster size

The BDEs of the first alkene ligand additions to the Ag_m^+ clusters ($m=1-13$ for C_2H_4 and $m=1-9$ for C_3H_6) are plotted as a function of silver cluster size (m) in Fig. 3. BDEs for the $\text{Ag}_{1,2}^+(\text{L})$ clusters were taken from previous work [27]. From Fig. 3, it is clear that the BDEs of the first ligand additions decrease as m increases. The Ag_6^+ and Ag_7^+ systems are exceptions to this trend. The BDEs for the loss of a ligand from $\text{Ag}_{6,7}^+(\text{L})$ are comparable to those reported for the $\text{Ag}_{2,3}^+$ systems. Some deviation from the trend is also observed for C_2H_4 additions to the larger silver clusters. The BDEs for loss of a ligand from $\text{Ag}_{12,13}^+(\text{C}_2\text{H}_4)$ are slightly larger than for the $\text{Ag}_{10,11}^+$ systems. However, the differences in the BDEs of these systems are quite small (less than 2 kcal/mol), and will therefore not be explicitly discussed.

In order to understand the observed bonding trend, the electron distributions of the Ag_m^+ clusters must be examined (Table 19). The strongest silver–alkene bond formed is observed for the monomer systems. Here, the $\pi(2p_y)^2$ electron density is donated from the alkene ligand to the unoccupied 5s orbital of Ag^+ . The amount of positive charge the first ligand encounters at the binding site is +1. For the dimer, a single electron occupies the $\sigma(5s)$ orbital of the cluster. The amount of positive charge that the first ligand encounters at a binding site is reduced to +0.5 due to symmetry. Each additional increase in the size of a silver cluster (by adding on Ag atom) results in one additional electron that is distributed in some manner about the atoms that comprise the cluster. The additional electron density usually reduces the amount of positive charge at the atomic center encountered by a ligand attempting to bind to the cluster. The result is a systematic decrease in the covalent interactions of the Ag_m^+ clusters with the alkene ligands as the cluster size (m) increases.

The explanation for why the Ag_6^+ and Ag_7^+ systems break from the trend can also be found by examination of Table 19. Ag_6^+ and Ag_7^+ are the first bare silver clusters to have 3-dimensional geometries. The onset of 3-dimensional conformations brings about an interesting shift in electron configuration. NBO indicates that the valence electron density is mainly distributed about the four atoms shown in red and green for Ag_6^+ and about atoms shown in red for Ag_7^+ . This leaves the two remaining Ag atoms of both clusters highly positively charged. The amount of positive charge encountered by a ligand binding to one these sites is intermediate between the Ag_2^+ and Ag_3^+ systems and leads to the relatively large BDEs of the first (and second) ligand additions to Ag_6^+ and Ag_7^+ . As with the $\text{Ag}_5^+(\text{L})_3$ clusters, calculations indicate that back-donation from Ag_6^+ and Ag_7^+ to the unoccupied $\pi^*(2p_y)$ orbitals of the alkene ligands also plays a role in the bonding. This contributes to the highly negative ΔS_T° values of these association reactions.

Although the structures of the larger Ag_m^+ clusters ($8 \leq m \leq 13$) are also 3-dimensional, no large concentration of

positive charge is found on the atoms of these clusters. Instead, the electron density of these clusters is distributed somewhat evenly about all the atoms, leading to the observed decline in the BDEs of the first ligand additions.

Information about the approach to bulk-phase properties of silver can also be extracted from the plots in Fig. 3. It is clear from the graphs that the BDEs of the first ligand additions to the clusters are asymptotically approaching some value. The energy required to remove a C₃H₆ and a C₂H₄ ligand from an Ag(1 1 0) surface has been measured to be approximately 12 kcal/mol [43] and 10 kcal/mol [44], respectively. For Ag₉⁺, the BDE for loss of the C₃H₆ ligand is still larger than the value for propene desorption from bulk silver. Likewise, the BDE for loss of C₂H₄ from Ag₁₃⁺ is also larger than the value for ethene desorption from bulk silver. However, the Ag_m⁺ systems are rapidly nearing these values by the time the 9th (13th) cluster is reached. This implies that the Ag_m⁺ clusters may arrive at their bulk-phase properties fairly quickly, most likely at sizes of tens of atoms rather than at sizes of hundreds or thousands of atoms. Although, deviations from the trend shown in Fig. 3 cannot be ruled out at some larger Ag_m⁺ cluster size.

6. Conclusions

1. Bond dissociation energies and association entropies were determined for sequential clustering of C₂H₄ ligands to Ag_m⁺ ($m = 3\text{--}13$) and of C₃H₆ ligands to Ag_m⁺ ($m = 3\text{--}9$). The manner in which the ligands bind is unique for each of the silver clusters and is governed by the electronic environment of the cluster.
2. Density functional theory calculations (B3LYP parameterization) yield BDEs in good agreement with experiment for the early ligand additions to the smaller Ag_m⁺ clusters ($m = 3\text{--}5$). The agreement becomes slightly worse for subsequent ligand additions to these clusters as well as for all ligand additions to the larger clusters, but trends in binding energy observed experimentally are all duplicated.
3. Additions of alkene ligands to Ag_m⁺(L)_n clusters where $n \leq m$ result in bonds having strong covalent character exemplified by electron donation from the $\pi(2p_y)^2$ orbital of the ligands into the 5s-comprised LUMO of the Ag_m⁺ clusters. In all systems studied, the location of the LUMO of a given Ag_m⁺ cluster directly correlates with the position of the Ag atom of the cluster having the highest partial positive charge. Additions of alkene ligands to Ag_m⁺(L)_n clusters where $n > m$ yield bonds that are essentially purely electrostatic (second solvation shell).
4. The binding energies of the first alkene ligand additions are plotted as a function of Ag_m⁺ cluster size. With the exception of the Ag_{6,7}⁺ clusters, the BDEs for loss of the ligand from the Ag_m⁺ clusters decrease as the size of the silver clusters increase. The trend is attributed to a reduction of the Ag_m⁺–alkene covalent interactions caused by dilution of the positive charge of the metal clusters. The trend also suggests that the binding energies of the Ag_m⁺ clusters relatively rapidly approach their bulk-phase values.

Acknowledgements

The support of the Air Force Office of Scientific Research under grants F 49620-01-1-0459 and F 49620-03-1-0046 is gratefully acknowledged. Additionally, M.J.M. would like to thank P. Weis and S. Chretien for helpful private communications regarding this work.

Appendix A. Supplementary data

Supplementary data associated with this article can be found, in the online version, at doi:10.1016/j.ijms.2005.12.028.

References

- [1] R.A.J. O'Hair, G.N. Khairallah, J. Cluster Sci. 15 (2004) 331.
- [2] M.M. Kappes, Chem. Rev. 88 (1988) 369.
- [3] M. Moskovits, Metal Clusters, Wiley, New York, 1986.
- [4] A.W. Castleman Jr., R.G. Keesee, Acc. Chem. Res. 19 (1986) 413.
- [5] M. Haruta, Catal. Today 36 (1997) 153.
- [6] A. Sanchez, S. Abbet, U. Heiz, W.D. Schneider, H. Hakkinen, R.N. Barnett, U. Landman, J. Phys. Chem. A 103 (1999) 9573.
- [7] S. Lee, C. Fan, T. Wu, S.L. Anderson, J. Am. Chem. Soc. 126 (2004) 5682.
- [8] K. Eller, H. Schwarz, Chem. Rev. 91 (1991) 1121.
- [9] M.B. Knickelbein, Annu. Rev. Phys. Chem. 50 (1999) 79.
- [10] B.S. Freiser (Ed.), Organometallic Ion Chemistry, Kluwer Academic Publishers, Dordrecht, The Netherlands, 1996.
- [11] D.H. Russell (Ed.), Gas Phase Inorganic Chemistry, Plenum, New York, 1989.
- [12] J.E. Bushnell, P.R. Kemper, P. Maitre, M.T. Bowers, J. Am. Chem. Soc. 116 (1994) 9710.
- [13] P.R. Kemper, P. Weis, M.T. Bowers, Int. J. Mass Spectrom. Ion Process. 160 (1997) 17.
- [14] M.J. Manard, J.E. Bushnell, S.L. Bernstein, M.T. Bowers, J. Phys. Chem. A 106 (2002) 10027.
- [15] T.H. Lee, K.M. Ervin, J. Phys. Chem. 98 (1994) 10023.
- [16] F. Meyer, Y.M. Chen, P.B. Armentrout, J. Am. Chem. Soc. 117 (1995) 4071.
- [17] B. Liang, L. Andrews, J. Phys. Chem. 104 (2000) 9156.
- [18] M.J. Manard, P.R. Kemper, M.T. Bowers, Int. J. Mass Spectrom. 228 (2003) 865.
- [19] D. Vardhan, R. Liyanage, P.B. Armentrout, J. Chem. Phys. 119 (2003) 4166; X.G. Zhang, P.B. Armentrout, J. Phys. Chem. A 107 (2003) 8904.
- [20] P. Weis, P.R. Kemper, M.T. Bowers, J. Phys. Chem. A 101 (1997) 8207.
- [21] Y.M. Chen, P.B. Armentrout, J. Phys. Chem. 99 (1995) 11424.
- [22] B.C. Guo, A.W. Castleman, Chem. Phys. Lett. 181 (1991) 16.
- [23] Q. Zhang, P.R. Kemper, M.T. Bowers, Int. J. Mass Spectrom. 210 (2001) 265.
- [24] P.A.M. van Koppen, M.T. Bowers, C.L. Haynes, P.B. Armentrout, J. Am. Chem. Soc. 120 (1998) 5704.
- [25] L. Benz, X. Tong, P. Kemper, Y. Lilach, A. Kolmakov, H. Metiu, M.T. Bowers, S.K. Buratto, J. Chem. Phys. 122 (2005) 081102; X. Tong, L. Benz, P. Kemper, H. Metiu, M.T. Bowers, S.K. Buratto, J. Am. Chem. Soc. 127 (2005) 13516.
- [26] M.J. Manard, P.R. Kemper, C.J. Carpenter, M.T. Bowers, Int. J. Mass Spectrom. 241 (2005) 99.
- [27] M.J. Manard, P.R. Kemper, M.T. Bowers, Int. J. Mass Spectrom. 241 (2005) 109.
- [28] M.J. Manard, P.R. Kemper, M.T. Bowers, J. Am. Chem. Soc. 127 (2005) 9994.
- [29] J.G. Serafin, A.C. Liu, S.R. Seyedmonir, J. Mol. Catal. A: Chem. 131 (1998) 157;

- D.J. Sajkowski, M. Boudart, *Catal. Rev.* 29 (1987) 325;
A.L. de Oliveira, A. Wolf, F. Schuth, *Catal. Lett.* 73 (2001) 157.
- [30] P.R. Kemper, M.T. Bowers, *J. Am. Soc. Mass Spectrom.* 1 (1990) 197.
- [31] P. Hohenberg, W. Kohn, *Phys. Rev. B* 136 (1964) B864;
W. Kohn, L.J. Sham, *Phys. Rev.* 140 (1965) 1133.
- [32] P.R. Kemper, J. Bushnell, G. von Helden, M.T. Bowers, *J. Phys. Chem.* 97 (1993) 52.
- [33] P.J. Stephens, F.J. Devlin, C.F. Chabalowski, M.J. Frisch, *J. Phys. Chem.* 98 (1994) 11623.
- [34] A.D. Becke, *J. Chem. Phys.* 98 (1993) 5648;
A.D. Becke, *Phys. Rev. A* 38 (1988) 3098.
- [35] M.J. Frisch, G.W. Trucks, H.B. Schlegel, G.E. Scuseria, M.A. Robb, J.R. Cheeseman, V.G. Zakrzewski, J.A. Montgomery Jr., R.E. Stratmann, J.C. Burant, S. Dapprich, J.M. Millam, A.D. Daniels, K.N. Kudin, M.C. Strain, O. Farkas, J. Tomasi, V. Barone, M. Cossi, R. Cammi, B. Mennucci, C. Pomelli, C. Adamo, S. Clifford, J. Ochterski, G.A. Petersson, P.Y. Ayala, Q. Cui, K. Morokuma, D.K. Malick, A.D. Rabuck, K. Raghavachari, J.B. Foresman, J. Cioslowski, J.V. Ortiz, A.G. Baboul, B.B. Stefanov, G. Liu, A. Liashenko, P. Piskorz, I. Komaromi, R. Gomperts, R.L. Martin, D.J. Fox, T. Keith, M.A. Al-Laham, C.Y. Peng, A. Nanayakkara, C. Gonzalez, M. Challacombe, P.M.W. Gill, B. Johnson, W. Chen, M.W. Wong, J.L. Andres, C. Gonzalez, M. Head-Gordon, E.S. Replogle, J.A. Pople, *Gaussian 03, Revision B.04*, Gaussian, Inc., Pittsburgh, PA, 2003.
- [36] M.M. Francl, W.J. Pietro, W.J. Hehre, J.S. Binkley, M.S. Gordon, D.J. Defrees, J.A. Pople, *J. Chem. Phys.* 77 (1982) 3654;
T. Clark, J. Chandrasekhar, G.W. Spitznagel, P.V. Schleyer, *J. Comput. Chem.* 4 (1983) 294;
R. Krishnan, J.S. Binkley, R. Seeger, J.A. Pople, *J. Chem. Phys.* 72 (1980) 650;
P.M.W. Gill, B.G. Johnson, J.A. Pople, M.J. Frisch, *Chem. Phys. Lett.* 197 (1992) 499.
- [37] P.J. Hay, W.R. Wadt, *J. Chem. Phys.* 82 (1985) 270;
W.R. Wadt, P.J. Hay, *J. Chem. Phys.* 82 (1985) 284;
P.J. Hay, W.R. Wadt, *J. Chem. Phys.* 82 (1985) 299.
- [38] Basis sets were obtained from the Extensible Computational Chemistry Environment Basis Set Database, Version 10/21/03, as developed and distributed by the Molecular Science Computing Facility, Environmental and Molecular Sciences Laboratory which is part of the Pacific Northwest Laboratory, P.O. Box 999, Richland, WA 99352, USA, and funded by the U.S. Department of Energy. The Pacific Northwest Laboratory is a multi-program laboratory operated by Battelle Memorial Institute for the U.S. Department of Energy under contract DE-AC06-76RLO 1830. Contact David Feller or Karen Schuchardt for further information.
- [39] P. Weis, T. Bierweiler, S. Gilb, M.M. Kappes, *Chem. Phys. Lett.* 355 (2002) 355.
- [40] A.E. Reed, L.A. Curtis, F. Weinhold, *Chem. Rev.* 88 (1988) 899, and references therein.
- [41] S. Chretien, M.S. Gordon, H. Metiu, *J. Chem. Phys.* 121 (2004) 3756;
S. Chretien, M.S. Gordon, H. Metiu, *J. Chem. Phys.* 121 (2004) 9925;
S. Chretien, M.S. Gordon, H. Metiu, *J. Chem. Phys.* 121 (2004) 9931.
- [42] H. Nishimura, H. Tawara, *J. Phys. B: At. Mol. Opt. Phys.* 27 (1994) 2063.
- [43] J. Pawela-Crew, R.J. Madix, *J. Chem. Phys.* 104 (1996) 1699.
- [44] C. Backx, C.P.M. de Groot, P. Biloen, W.M.H. Sachtler, *Surf. Sci.* 128 (1983) 81;
C. Backx, C.P.M. de Groot, P. Biloen, *Appl. Surf. Sci.* 6 (1980) 256.